ARTICLE

Near-UV Photodissociation Dynamics of Thiomethoxy Radical via $\widetilde{A}^2A_1$ State: H-atom Product Channel[†]

Xian-feng Zheng[a,b], Yu Song[a], Jing-ze Wu[a], Jing-song Zhang[a*]

a. Department of Chemistry, Air Pollution Research Center, University of California, Riverside, CA 92521, USA;
b. Department of Physics, Anhui Normal University, Wuhu 241000, China

(Dated: Received on June 2, 2007; Accepted on July 4, 2007)

Photodissociation dynamics of jet-cooled thiomethoxy radical (CH_3S) via the $\widetilde{A}^2A_1 \leftarrow \widetilde{X}^2E$ transition is investigated near 352 nm. The H-atom product channel is observed directly for the first time by H-atom product yield spectrum and photofragment translational spectroscopy. The $2^1 3^2$ vibrational level of the $\widetilde{A}^2A_1$ state dissociates to the $H+H_2CS$ products. The $H+H_2CS$ product translational energy release is modest and peaks around 33 kJ/mol; the H-atom angular distribution is isotropic. The dissociation mechanism is consistent with internal conversion of the excited $\widetilde{A}^2A_1$ state to the $\widetilde{X}^2E$ ground state and subsequent unimolecular dissociation on the ground state to the $H+H_2CS$ products.

Key words: Photodissociation dynamics, Thiomethoxy radical

I. INTRODUCTION

The thiomethoxy radical (CH_3S) is an important intermediate in atmospheric oxidation of naturally occurring sulfur species such as dimethyl sulfide (CH_3SCH_3) and dimethyl disulfide (CH_3SSCH_3) [1-4]. The spectroscopy of the thiomethoxy radical has been extensively studied, including electronic absorption [5,6] and emission spectra [7], microwave spectroscopy [8], photoelectron and photodetachment spectroscopy [9-11], laser-induced fluorescence (LIF) [12-15] and fluorescence depletion spectroscopy (FDS) [16], photofragment yield spectroscopy [17], and four-wave mixing spectroscopy [18,19]. These studies have provided information on the geometric and spectral parameters of both the ground state $\widetilde{X}^2E$ and the first electronic excited state $\widetilde{A}^2A_1$. In particular, the $\widetilde{A}^2A_1$ state and the $\widetilde{A}^2A_1 \leftarrow \widetilde{X}^2E$ transition in the near ultraviolet (UV) region have been well characterized by fluorescence [12-16], photofragment yield [17], and four-wave mixing spectroscopy [18,19]. Vibrationally resolved spectra of the $\widetilde{A}^2A_1 \leftarrow \widetilde{X}^2E$ band show predominant progressions in the symmetric C−S stretch (ν_3) and CH_3 umbrella (ν_2) modes, along with other combination states involving the symmetric CH_3 stretching (ν_1) and asymmetric CH_3 stretching (ν_4) modes [12-19]. The rotationally resolved spectrum indicates that the C−S bond is lengthened and the HCS bond angle decreases in the $\widetilde{A}^2A_1$ state [14], consistent with the predominant C−S stretch (ν_3) progression in the $\widetilde{A}^2A_1 \leftarrow \widetilde{X}^2E$ band. The radiative lifetime of the $\widetilde{A}$ state vibrational levels above 27321 cm^{-1} (>800 cm^{-1} above the $\widetilde{A}$ state origin) decreases significantly, and no emission is observed above 28016 cm^{-1} (1490 m^{-1} above the $\widetilde{A}$ origin). This is attributed to predissociation of the $\widetilde{A}$ state and limits LIF measurements to lower vibrational levels of the $\widetilde{A}$ state. The higher $\widetilde{A}$ state vibrational levels (mainly the higher ν_3 states and ν_2 and ν_3 combination states, up to ∼5200 cm^{-1} above the $\widetilde{A}$ state origin) are observed by fluorescence depletion spectroscopy [16], four-wave mixing spectroscopy [18,19], and photofragment yield spectroscopy [17].

The thiomethoxy radical has also been studied by theoretical methods, and several *ab initio* calculations have been carried out to characterize both the ground and the excited electronic states of the CH_3S radical [20-24]. Figure 1 depicts the potential energy surfaces (PES's) diagram of CH_3S along the C−S and the C−H dissociation coordinate, based on the theoretical calculations of Hsu *et al.* [22] and Cui *et al.* [23]. The $\widetilde{X}^2E$ ground state correlates asymptotically with the $CH_3(\widetilde{X}^2A_1'')+S(^3P_J)$ products and the $H+H_2CS(\widetilde{X}^1A_1)$ products. The first electronic excited state $\widetilde{A}^2A_1$ correlates asymptotically with the $CH_3(\widetilde{X}^2A_2'')+S(^1D)$ product channel and is crossed by three repulsive states, $^4A_2$, ^4E, and $\widetilde{B}^2A_2$. These three repulsive states induce predissociation in the $\widetilde{A}^2A_1$ state and correlate to the ground state products $CH_3(\widetilde{X}^2A_2'')+S(^3P_J)$. Photodissociation of the methoxy radical family CX_3Y (X=H, F; Y=O, S) from the $\widetilde{A}^2A_1$ state has been studied using *ab initio* MO calculations by Cui *et al.* [23]. Three dissociation channels have been considered:

[†]Part of the special issue "Cun-hao Zhang Festschrift".
*Author to whom correspondence should be addressed. E-mail: jingsong.zhang@ucr.edu, Fax: 1-951-827-4713

$$CX_3Y+h\nu\rightarrow CX_3+Y \quad (1)$$
$$\rightarrow CX_2+YX \quad (2)$$
$$\rightarrow CX_2Y+X \quad (3)$$

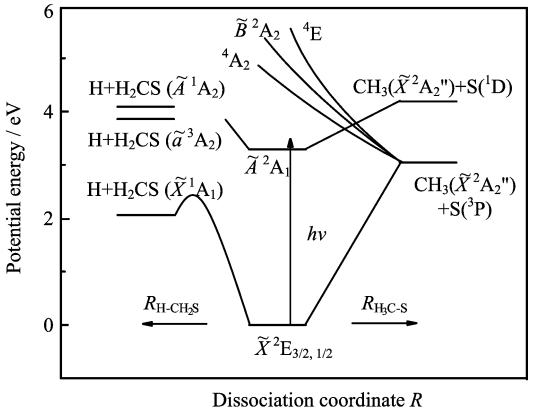

FIG. 1 Schematics of potential energy diagram of the CH_3S system. The dissociation mechanism leading to the CH_3+S products is shown along the C−S dissociation coordinate (in C_{3v}). The dissociation mechanism of the H+H_2CS channel is shown along the C−H dissociation coordinate. The energetics are based on theoretical calculations (from Ref.[22,23]) and experimental values (from Ref.[16,17]).

The dissociation dynamics on the first excited state $\widetilde{A}^2A_1$ of CH_3O and CH_3S have been examined experimentally by Neumark and co-workers using photofragment translational spectroscopy [17,25]. For CH_3O, three channels are identified: (i) predissociation to CH_3+O, (ii) isomerization and dissociation to CH_2+OH, and (3) predissociation to H+H_2CO, with (i) being the dominant channel [25]. In CH_3S, only one major channel, $CH_3(\widetilde{X}^2A_2'')$+S($^3P_J$), is observed [17]. In both CH_3O and CH_3S, the photofragment yield spectra for the $\widetilde{A}^2A_1\leftarrow\widetilde{X}^2E$ electronic transition show resolved vibrational progressions of C−O(S) stretch and the associated combination bands [17,25]. In CH_3S, the C−S stretch mode ν_3 extends from 3^2 to 3^{15} (for $\widetilde{A}^2A_1\leftarrow\widetilde{X}^2E_{3/2}$), and the ν_2 and ν_3 combination band extends from 2^13^3 to 2^13^{12}, while the 2^13^1 and 2^13^2 bands were not observed in this experiment [17]. In later studies, the radiative and nonradiative decays of the $\widetilde{A}^2A_1$ state CH_3S are investigated using LIF and FDS by Miller and co-workers [16] and four-wave mixing spectroscopy by Lee and co-workers [18,19]. With the increase of energy, the lifetimes of the 3^ν and 2^13^ν bands decrease and the homogeneous linewidths increase significantly, indicating mode specificity in the nonradiative processes and the ν_3 mode being the promoting mode for dissociation (to the CH_3+S(^3P_J) products). The 3^2 and 2^13^1 bands are observed by LIF with short lifetimes of 250 and 60 ns [15,16]. The 2^13^2 band is observed only in the FDS and four-wave mixing spectroscopy but not in LIF [16,18], and thus is completely dark, with a lifetime in the range of 10 ps to 10 ns [16]. All these three vibronic states are strongly predissociative, and comparison of the natural lifetimes of these levels with that of the $\widetilde{A}^2A_1$ state origin indicates that more than 80%, 94%, and 99% of the CH_3S radicals excited into the 3^2, 2^13^1, and 2^13^2 levels, respectively, undergo nonradiative decays [16]. However, these three states do not fragment into the CH_3+S(^3P_J) products, since the 3^2, 2^13^1, and 2^13^2 bands are not observed in the CH_3+S(^3P_J) product yield spectrum by Neumark and co-workers [17]. It is then suggested by Miller and co-workers that in the near-UV excitation region of less than three quanta of ν_3, there might be another dissociation channel (likely the H+H_2CS product channel) [16]. Note that both the CH_2+SH and the H_2CS+H product channels are thermodynamically possible dissociation pathways. The H+H_2CS product channel in the near-UV photodissociation of CH_3S via the $\widetilde{A}^2A_1$ state has not been directly observed before. It should be pointed out that H-atom product is observed at higher UV energy in the 213-220 nm photodissociation of CH_3S in the secondary photolysis of CH_3SH [26]. At this high energy, CH_3S is excited to the repulsive $\widetilde{B}^2A_2$ state via the $\widetilde{B}^2A_1\leftarrow\widetilde{X}^2E$ transition, and H_2CS associated with the main H-atom elimination channel is believed to be produced in the electronically excited $\widetilde{A}^1A_2$ state [26].

In the present study, the dynamics of H-atom production from photodissociation of the jet-cooled CH_3S radical via the 2^13^2 level of the $\widetilde{A}^2A_1$ state near 352 nm is studied using resonance-enhanced multiphoton ionization (REMPI) technique, photofragment yield spectroscopy, and high-n Rydberg time-of-flight technique (HRTOF). The H atom is detected by 1+1 REMPI (VUV at Lyman-α+UV at 364 nm), and the H-atom photofragment yield spectrum is obtained as the action spectrum by scanning the near-UV photolysis radiation around the 2^13^2 vibronic transition. The H-atom photofragment translational spectroscopy is obtained by HRTOF as described in our previous papers [27-30]. We report the first direct observation of the H+H_2CS product channel from the 2^13^2 level of CH_3S ($\widetilde{A}^2A_1$) and provide more insights into the predissociative dynamics of the CH_3S $\widetilde{A}^2A_1$ state.

II. EXPERIMENTS

The HRTOF technique and experimental setup have been described previously [27-30]. A pulsed CH_3S radical beam was generated by photolyzing dimethyl disulfide (CH_3SSCH_3) ($\geq$99.0%, Aldrich) seeded in He ($\sim$2% at a total pressure of 120 kPa) with the 193-nm radiation of an ArF excimer laser that was focused in front of the pulse nozzle. The CH_3S radicals produced from the photolysis were entrained in the seeded beam and subsequently cooled by supersonic expansion. The radical beam was collimated at 2.8 cm downstream by

DOI:10.1088/1674-0068/20/04/377-382

a 1-mm diameter skimmer into a high-vacuum chamber; at 4.6 cm further downstream the skimmer, the CH_3S radical beam crossed with a slightly focused near-UV photolysis laser radiation (∼352 nm, 4-7 mJ/pulse, linewidth $\leq$0.3 cm^{-1}). The absolute photolysis laser wavelength was monitored by a wavemeter (Burleigh WA-4500). The polarization of the photolysis radiation was rotated by a Fresnel-Rhomb achromatic $\lambda/2$ plate for product angular distribution measurements. The H atoms produced from the CH_3S photodissociation were tagged by two-color resonant excitation (121.53 nm+366.36 nm), i.e., from 1^2S to 2^2P via the H-atom Lyman-α transition and then further to a high-n Rydberg state. A small fraction of the radiatively metastable Rydberg H atoms drifted with their nascent velocities toward a microchannel plate (MCP) detector, and were field-ionized in front of the detector and detected. The flight length was 37.1 cm, which was calibrated by HBr photodissociation (with the spin-orbit splitting of $Br(^2P_{3/2})$ and $Br(^2P_{1/2})$). The ion signals were amplified by a fast pre-amplifier, and the H-atom TOF spectra were recorded and averaged using a multichannel scaler. The H-atom TOF spectra were typically accumulated with 10^5 laser firings.

The H-atom photofragment yield spectrum (action spectrum) is obtained by collecting H-atom product REMPI signals as a function of photolysis wavelength. The REMPI experiment was conducted in the same HRTOF instrument, and the photolysis and REMPI ionization lasers were the same as in the HRTOF experiment. Upon photodissociation by the near-UV laser radiation around 352 nm, the product H atoms were detected by 1+1 REMPI, with one Lyman-α photon resonantly exciting the H atom from 1^2S to 2^2P and the UV photon at ∼364 nm ionizing the H atom. The photolysis and REMPI probe laser delay time was fixed at 20 ns. The H^+ ions were extracted and accelerated in a linear TOF mass spectrometer, and were detected by the MCP detector. The mass-resolved ion current signal (at m/z=1, H^+) was preamplified and input into a Boxcar averager (SRS 250). The typical scanning rate of the photolysis laser was 0.01 nm/s. Typically 100 laser shots were averaged at each wavelength step, and the averaged signal was input to the computer data acquisition system. Three types of REMPI spectra were obtained: (i) the 193-nm radiation on (for CH_3S radical production) and photolysis on (for CH_3S radical photodissociation), (ii) the 193-nm radiation on and photolysis off, and (iii) the 193-nm radiation off and photolysis on. Only in (i), the $2^1 3^2$ vibronic transition was observed in the REMPI experiment. The photofragment yield spectrum reported in the following section is the net H-atom REMPI signals with the background from (ii) and (iii) removed. No attempt was made to normalize the photofragment yield spectrum with the photolysis laser power, which is essentially constant in the small scanning range.

III. RESULTS AND DISCUSSION

The H-atom photofragment yield spectrum in the vicinity of the $2^1 3^2$ band is shown in Fig.2. The spectrum shows the net H^+ signal from photodissociation of CH_3S, which is obtained from the spectrum with both the 193-nm radiation on and photolysis on minus the background with the 193-nm radiation on and photolysis off and with the 193-nm radiation off and photolysis on. The observed peak position of the $2^1 3^2$ band is in excellent agreement with that reported in the previous FDS and four-wave mixing spectroscopy studies [16,18]. This H-atom yield spectrum provides the first direct evidence for the $H+H_2CS$ dissociation channel in the near-UV photodissociation of the $2^1 3^2$ band of $CH_3S(\widetilde{A}^2A_1)$. At 28450 cm^{-1}, the 3^5 peak is expected with higher intensity than the $2^1 3^2$ peak, based on the LIF, four-wave mixing, and photofragment yield spectra; however, the 3^5 peak is not observed in the H-atom yield spectrum in Fig.2. The H-atom dissociation channel appears to depend on the $\widetilde{A}^2A_1$ state vibrational modes, indicating mode specificity in the dissociation. The H-atom product channel appears only at less than three quanta of ν_3 in the $\widetilde{A}^2A_1$ state, and at higher ν_3 levels, which approach the crossing seams between the $\widetilde{A}^2A_1$ state and the three repulsive states, the $CH_3+S(^3P_J)$ channel competes strongly and becomes predominant.

TOF spectra of the H-atom product in the photodissociation of the CH_3S radical are recorded near the $2^1 3^2$ band around 352 nm (Fig.3). For background subtraction, two types of TOF spectra have been taken: (i) full spectrum, with both the 193 nm radiation on (for CH_3S radical production) and the near-UV photolysis radiation on, plus the Rydberg atom tagging probe laser radiations (121.6 nm+366.3 nm); and (ii) precursor background spectrum, with the 193 nm radiation off but the near-UV photolysis radiation on, plus the probe laser

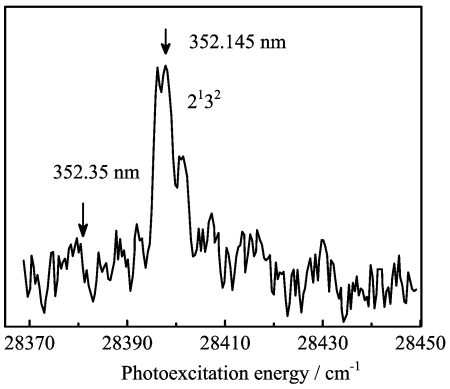

FIG. 2 H-atom product yield spectrum as a function of photolysis excitation energy in the vicinity of the $2^1 3^2$ level of $\widetilde{A}^2A_1$. The H atom is detected by 1+1 REMPI (VUV 121.6 nm+UV 364 nm). The arrows indicate the photolysis energies where the HRTOF spectra are taken.

DOI:10.1088/1674-0068/20/04/377-382

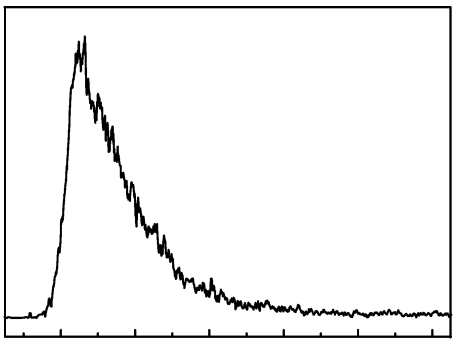

FIG. 3 H-atom TOF spectrum of CH_3S photodissociation via the $2^1 3^2$ level of $\widetilde{A}^2A_1$ at 352.145 nm. The spectrum is obtained as the net signals with the 193 nm photolysis laser (for radical production) on minus off. The polarization vector of the 352.145 nm photodissociation radiation is perpendicular (θ=90°) to the TOF axis. The H-atom product angular distribution is isotropic with respect to θ.

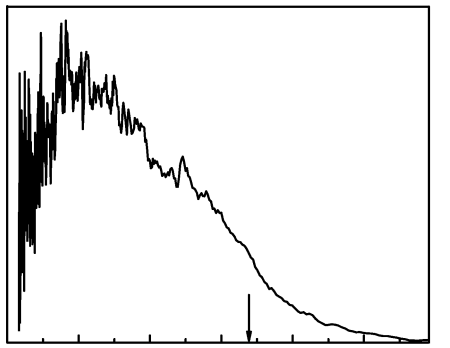

FIG. 4 Center-of-mass $H+H_2CS$ product translational energy distribution, $P(E_T)$, from 352.145 nm photodissociation of CH_3S. The $P(E_T)$ distribution is converted from the TOF spectrum in Fig.3. The maximum translational energy of the products from one-photon photodissociation of CH_3S at 352.145 nm is indicated by the arrow.

radiation. The net spectrum obtained by removing the background in spectrum (ii) (with the 193 nm photolysis laser off) from spectrum (i) (with the 193 nm laser on) represents the H-atom product signals from photodissociation of the CH_3S radical by the near-UV photolysis radiation and possibly by the 121.6 nm Lyman-α probe radiation (see discussion in the following).

The net H-atom TOF spectrum of the jet-cooled CH_3S photodissociation at 352.145 nm is transformed to product center-of-mass (CM) translational energy distribution $P(E_T)$ [28,31] and is shown in Fig.4. The C−H bond dissociation energy of CH_3S in $CH_3S(\widetilde{X}^2E)\rightarrow H_2CS(\widetilde{X}^1A_1)+H$ is 198.7±7.5 kJ/mol [17]. With the near-UV photolysis radiation at 352.145 nm, the maximum CM translational energy of the $H+H_2CS(\widetilde{X}^1A_1)$ products is 141.0±7.5 kJ/mol, which is indicated by the arrow in Fig.4. The translational energy release is modest and not repulsive. The translational energy distribution $P(E_T)$ is broad and peaks at ∼33 kJ/mol, indicating rovibrationally excited $H_2CS(\widetilde{X}^1A_1)$ product. The $P(E_T)$ distribution of the $H+H_2CS$ channel is very different from that of the $CH_3(\widetilde{X}^2A_2'')+S(^3P_J)$ product channel. For the $CH_3(\widetilde{X}^2A_2'')+S(^3P_J)$ product channel, the $P(E_T)$'s peak near the maximum available energy [17], and the translational energy release is highly repulsive, consistent with rapid dissociation on the repulsive states $^4A_2$, ^4E, and $\widetilde{B}^2A_2$ after curve crossing and predissociation of the $\widetilde{A}^2A_1$ state (Fig.1). The small translational energy release in the $P(E_T)$ of the $H+H_2CS$ channel, however, suggests that the $H+H_2CS$ channel occurs via a different dissociation mechanism. The mechanism that is consistent with $P(E_T)$ of the $H+H_2CS$ channel is unimolecular dissociation of highly vibrationally excited ground state $CH_3S(\widetilde{X}^2E)$ following internal conversion from the electronically excited $\widetilde{A}^2A_1$ state. It is unlikely for the excited $\widetilde{A}^2A_1$ state to dissociate directly to the $H+H_2CS$ products. The theoretical study by Cui *et al.* shows that the state leads to H and the excited state $H_2CS(\widetilde{a}^3A')$, which is at higher energy [23]. This higher energy $H+H_2CS(\widetilde{a}^3A')$ channel is closed in the near-UV photodissociation of CH_3S in the work.

A portion of the $P(E_T)$ distribution of the $H+H_2CS$ channel is beyond the energy limit of one-photon dissociation by the near-UV photolysis radiation (Fig.4). Several possibilities have been examined. The signals are shown to depend linearly on the near-UV photolysis laser power and the Rydberg probe laser power; therefore the fast signals are not from multiphoton processes of the photolysis or Rydberg laser. CH_3 is another product from the near-UV photodissociation of CH_3S, and its photodissociation by the 121.6 nm probe laser could generate some fast H-atom signals. However, a separate experiment indicates no H-atom signals from the 121.6 nm photolysis of CH_3 (produced from 193 nm photodissociation of acetone). The fast component seems to have a stronger (more than linear) power dependence on the 121.6 nm radiation. It is plausible that they come from 121.6 nm photodissociation of the CH_3S radical or the H_2CS product generated in the near-UV dissociation of CH_3S. The majority of the H-atom signals (the slow H atoms) are believed to be from one-photon photodissociation of CH_3S by the near-UV photolysis radiation. The upper limit of the average product translational energy in the one-photon photodissociation of CH_3S at 352.145 nm is estimated to be ∼67 kJ/mol (Table I).

The angular distribution of the H-atom product from CH_3S is studied with the photolysis laser polarization parallel and perpendicular to the flight path, respectively. The TOF spectra at the parallel and perpendicular polarization are of the same intensity and shape,

DOI:10.1088/1674-0068/20/04/377-382

TABLE I Product energetics and angular distribution of the H+CH_2S channel in the CH_3S photodissociation via the $\widetilde{A}^2A_1$ $2^1 3^2$ level at 352.145 nm

Photon energy/(kJ/mol)	339.7
$E_{\rm avail}$/(kJ/mol)	141.0±7.5
$\langle E_T\rangle$/(kJ/mol)	≤67.0
$\langle f_T\rangle$	≤0.47
Anisotropy parameter β	∼0

indicating an isotropic H-atom product angular distribution. The photofragment angular distribution can be described by $I(\theta)=(1/4\pi)[1+\beta P_2(\cos\theta)]$, where β is the anisotropy parameter ($-1\leq\beta\leq2$), θ is the angle between the electric vector of the polarized laser radiation E and the recoiling velocity vector of the H atom product (the direction of detection or the TOF axis), and $P_2(\cos\theta)$ is the second Legendre polynomial [32]. The anisotropy parameter for the H-atom product channel in the photodissociation of CH_3S via the $2^1 3^2$ band is $\beta\approx0$ (Table I). The isotropic angular distribution implies that the H atom elimination in CH_3S via the $2^1 3^2$ band occurs on a time scale longer than the rotational period (∼ps) of the CH_3S parent. This dissociation time scale, along with the small kinetic energy release and the shape of the $P(E_{\rm T})$ distribution, is consistent with unimolecular dissociation of the ground state $CH_3S(\widetilde{X}^2E)$ to H+H_2CS following the internal conversion from the $\widetilde{A}^2A_1$ state of CH_3S.

The H+H_2CS channel in the near-UV photodissociation of CH_3S via the lower vibrational levels 3^2, $2^1 3^1$, and $2^1 3^2$ of the $\widetilde{A}^2A_1$ state was first suggested by Miller and co-workers in their fluorescence depletion study [16]. Their conclusion was based on two facts: (i) the 3^2 and $2^1 3^1$ bands in the LIF spectra have short lifetime, and the $2^1 3^2$ band is missing in the LIF spectrum and is observed only in the fluorescence depletion and four-wave mixing spectra [16,18], indicating fast nonradiative decay processes for these bands; and (ii) the 3^2, $2^1 3^1$, and $2^1 3^2$ bands were not observed in the CH_3+$S(^3P_J)$ product yield spectrum by Neumark and co-workers [17]. These observations imply that other nonradiative decay processes (other than the CH_3+S channel) should be responsible for the fast decay of the 3^2, $2^1 3^1$, and $2^1 3^2$ levels of the $\widetilde{A}^2A_1$ state CH_3S, and the H+H_2CS channel is the likely decay process for these three states. Indeed, this current study observes directly for the first time the H+H_2CS channel in the near-UV photodissociation of CH_3S via the $2^1 3^2$ levels of the $\widetilde{A}^2A_1$ state, and characterizes the translational energy release of the H+H_2CS products.

The general picture of the near-UV photodissociation of CH_3S via the $\widetilde{A}^2A_1$ state is as follows (Fig.1). Upon excitation to the $\widetilde{A}^2A_1$ state, two nonradiative decay processes, in addition to the radiative decay of the $\widetilde{A}^2A_1$ state, are involved. At energy above two quanta of ν_3, the $\widetilde{A}^2A_1$ state couples efficiently with and predissociates via the three repulsive states $^4A_2$, ^4E, and $\widetilde{B}^2A_2$, leading to the CH_3+$S(^3P_J)$ products with repulsive energy release [17]. The predissociation process is mode selective, and the C−S stretch ν_3 of the $\widetilde{A}^2A_1$ state is shown to be the promoting mode for the predissociation [16-19]. In the region of two or less quanta of ν_3 excitation, which is near the minimum of the PES of the $\widetilde{A}^2A_1$ state and further away from the crossing seams with the three repulsive states, the predissociation via the three repulsive states is less efficient, and another nonradiative process, the internal conversion of the $\widetilde{A}^2A_1$ state to the ground state $\widetilde{X}^2E$ and subsequent unimolecular dissociation to H+H_2CS, becomes significant [16]. This second channel occurs in a unique energy window. It is below the crossing seams between the $\widetilde{A}^2A_1$ state and the three repulsive states and is thus competitive with the predissociation to CH_3+$S(^3P_J)$, while it is also above the minimum of the $\widetilde{A}^2A_1$ state and in a region where the $\widetilde{A}^2A_1$ state couples efficiently with the ground state $\widetilde{X}^2E$ to compete with the radiative decay (where the lowest vibronic levels of the $\widetilde{A}^2A_1$ state have lifetimes of ∼1000 ns). The nature of the internal conversion mechanism is not clear yet, but in the region of the 3^2, $2^1 3^1$, and $2^1 3^2$ levels of the $\widetilde{A}^2A_1$ state, the coupling between the excited state $\widetilde{A}^2A_1$ and the ground state $\widetilde{X}^2E$ should be stronger than the predissociation of the $\widetilde{A}^2A_1$ state and its spin-orbit couplings with the three repulsive states $^4A_2$, ^4E, and $\widetilde{B}^2A_2$. Further theoretical study can help reveal more insights. After the internal conversion of the $\widetilde{A}^2A_1$ to the ground state $\widetilde{X}^2E$, the vibrationally hot CH_3S radical undergoes unimolecular dissociation to the H+$H_2CS(\widetilde{X}^1A_1)$ products. Note that the one-photon energy of 352.145 nm could produce only the ground state H_2CS ($\widetilde{X}^1A_1$) product. The $P(E_{\rm T})$ distribution with small translational energy release is typical for a unimolecular dissociation process from the ground state hot radical, and the isotropic H-atom product angular distribution also supports this mechanism [33,34]. The $P(E_{\rm T})$ distribution peaks at ∼33 kJ/mol, indicating an exit channel barrier of the similar magnitude [33,34]. Note that in the similar system CH_3O, a 16.7 kJ/mol exit channel barrier for the H+H_2CO product channel has been suggested [35].

IV. CONCLUSION

Photodissociation dynamics of the jet-cooled CH_3S radical via the $\widetilde{A}^2A_1\leftarrow\widetilde{X}^2E$ transition is investigated near 352 nm. The H+$H_2CS(\widetilde{X}^1A_1)$ product channel in the photodissociation of CH_3S via the $2^1 3^2$ level of $\widetilde{A}^2A_1$ at 352.145 nm is observed directly for the first time by H-atom product yield spectrum and photofragment translational spectroscopy. The H+$H_2CS(\widetilde{X}^1A_1)$

DOI:10.1088/1674-0068/20/04/377-382

product translational energy release is modest and peaks at ∼33 kJ/mol. The H-atom product angular distribution is isotropic. The photodissociation mechanism is consistent with internal conversion of the excited $\widetilde{A}^2A_1$ state to the $\widetilde{X}^2E$ ground state and subsequent unimolecular dissociation on the ground state $\widetilde{X}^2E$ to the $H+H_2CS(\widetilde{X}^1A_1)$ products. The $H+H_2CS(\widetilde{X}^1A_1)$ exit channel barrier is on the order of 33 kJ/mol.

V. ACKNOWLEDGMENT

This work was supported by the US National Science Foundation (CHE-0416244).

[1] R. J. Charlson, J. E. Lovelock, M. O. Andreae, and S. G. Warren, Nature **326**, 655 (1987).
[2] T. S. Bates, B. K. Lamb, A. Guenther, J. Dignon, and R. E. Stoiber, J. Atmos. Chem. **14**, 315 (1992).
[3] A. R. Ravishankara, Y. Rudich, R. Talukdar, and S. B. Barone, Philos. Trans. R. Soc. London B **352**, 171 (1997).
[4] G. S. Tyndall and A. R. Ravishankara, Int. J. Chem. Kinet. **23**, 483 (1991).
[5] A. B. Callear, J. Connor, and D. R. Dickson, Nature **221**, 1238 (1969).
[6] A. B. Callear and D. R. Dickson, Trans. Faraday Soc. **66**, 1987 (1970).
[7] K. Ohbayashi, H. Akimoto, and I. Tanaka, Chem. Phys. Lett. **52**, 47 (1977).
[8] Y. Endo, S. Saito, and E. Hirota, J. Chem. Phys. **85**, 1770 (1986).
[9] P. C. Engelking, G. B. Ellison, and W. C. Lineberger, J. Chem. Phys. **69**, 1826 (1978).
[10] B. K. Janousek and J. I. Brauman, J. Chem. Phys. **72**, 694 (1980).
[11] S. Moran and G. B. Ellison, J. Phys. Chem. **92**, 1794 (1988).
[12] M. Suzuki, G. Inoue, and H. Akimoto, J. Chem. Phys. **81**, 5405 (1984).
[13] G. Black and L. E. Jusinski, J. Chem. Soc. Faraday Trans. **82**, 2143 (1986).
[14] Y. C. Hsu, X. M. Liu, and T. A. Miller, J. Chem. Phys. **90**, 6852 (1989).
[15] S. Y. Chiang and Y. P. Lee, J. Chem. Phys. **95**, 66 (1991).
[16] M. B. Pushkarsky, B. E. Applegate, and T. A. Miller, J. Chem. Phys. **113**, 9649 (2000).
[17] R. T. Bise, H. Choi, H. B. Pedersen, D. H. Mordaunt, and D. M. Neumark, J. Chem. Phys. **110**, 805 (1999).
[18] C. P. Liu, Y. Matsuda, and Y. P. Lee, J. Chem. Phys. **119**, 12335 (2003).
[19] C. P. Liu, S. A. Reid, and Y. P. Lee, J. Chem. Phys. 122 (2005).
[20] R. Fournier and A. E. Depristo, J. Chem. Phys. **96**, 1183 (1992).
[21] L. A. Curtiss, R. H. Nobes, J. A. Pople, and L. Radom, J. Chem. Phys. **97**, 6766 (1992).
[22] C. W. Hsu, C. L. Liao, Z. X. Ma, P. J. H. Tjossem, and C. Y. Ng, J. Chem. Phys. **97**, 6283 (1992).
[23] Q. Cui and K. Morokuma, Chem. Phys. Lett. **263**, 54 (1996).
[24] A. V. Marenich and J. E. Boggs, J. Chem. Theo. Comput. **1**, 1162 (2005).
[25] D. L. Osborn, D. J. Leahy, and D. M. Neumark, J. Phys. Chem. A **101**, 6583 (1997).
[26] S. H. S. Wilson, M. N. R. Ashfold, and R. N. Dixon, J. Chem. Phys. **101**, 7538 (1994).
[27] L. Schnieder, W. Meier, K. H. Welge, M. N. R. Ashfold, and C. M. Western, J. Chem. Phys. **92**, 7027 (1990).
[28] K. S. Xu, G. Amaral, and J. S. Zhang, J. Chem. Phys. **111**, 6271 (1999).
[29] G. Amaral, K. S. Xu, and J. S. Zhang, J. Chem. Phys. **114**, 5164 (2001).
[30] W. D. Zhou, Y. Yuan, S. P. Chen, and J. S. Zhang, J. Chem. Phys. **123** (2005).
[31] J. Zhang, M. Dulligan, and C. Wittig, J. Phys. Chem. **99**, 7446 (1995).
[32] R. N. Zare, Mol. Photochem. **4**, 1 (1972).
[33] D. L. Osborn, H. Choi, D. H. Mordaunt, R. T. Bise, D. M. Neumark, and C. M. Rohlfing, J. Chem. Phys. **106**, 3049 (1997).
[34] D. H. Mordaunt, D. L. Osborn, and D. M. Neumark, J. Chem. Phys. **108**, 2448 (1998).
[35] A. Geers, J. Kappert, F. Temps, and J. W. Wiebrecht, J. Chem. Phys. **99**, 2271 (1993).

DOI:10.1088/1674-0068/20/04/377-382